

## Signature of chaos in high-lying doubly excited states of the helium atom

Anh-Thu Le,<sup>1,\*</sup> Toru Morishita,<sup>2</sup> X.-M. Tong,<sup>1</sup> and C. D. Lin<sup>1</sup>

<sup>1</sup>*Department of Physics, Cardwell Hall, Kansas State University, Manhattan, Kansas 66506, USA*

<sup>2</sup>*Department of Applied Physics and Chemistry, The University of Electro-Communications 1-5-1 Chofu-ga-oka, Chofu-shi, Tokyo 182-8585, Japan*

(Received 10 June 2005; published 30 September 2005)

We examined nearest-neighbor spacing (NNS) statistics in doubly excited states of helium near the double ionization threshold. Using the Brody parameter  $q$  to measure the NNS distribution between the regular Poisson distribution ( $q=0$ ) and the chaotic Wigner distribution ( $q=1$ ), we showed that for levels near the  $N=20$  threshold of  $\text{He}^+$ , or at about 0.13 eV below the double ionization threshold, the NNS distribution has  $q=0.66$ . The result shows the slow approach of the NNS of helium energy levels towards the Wigner distribution vs the excitation energy. Using an  $s$ -wave model where the angular momentum of each electron is restricted to zero, we also examined the NNS for levels up to the  $N=30$  threshold of  $\text{He}^+$ . We showed the gradual increase in  $q$  as the excitation energy is increased. To generate the theoretical data needed for the NNS analysis, we have used the hyperspherical close-coupling method, with the recently proposed diabaticization of potential curves and the truncation of channels, to greatly reduce the complexity in the calculation. We also investigated the dependence of  $q$  vs the nuclear charge in the same scaled energy region, and for different symmetries, to assess their relation with the rate of approaching the  $q=1$  Wigner distribution.

DOI: [10.1103/PhysRevA.72.032511](https://doi.org/10.1103/PhysRevA.72.032511)

PACS number(s): 31.10.+z, 31.25.Jf, 31.15.Ja, 05.45.Mt

### I. INTRODUCTION

It has been known since the work of Poincaré that, within a certain range of parameters, any given nonlinear classical dynamic system with at least three-dimensional phase space (assuming no additional constants of motion) is chaotic. In quantum physics, chaos, or quantum chaos, is not easily defined. A great deal has been done by comparing the model quantum systems with classical analogs, e.g., stadium and Sinai's billiard. The result is that some criteria have been established for quantum systems that would indicate whether the corresponding classical system be ordered or chaotic. One of such criteria is the statistical study of the spectra. For this, one distinguishes the local properties from the global properties of the spectra of a quantum system. For the latter, for example, one can speak of the density of levels vs the excitation energy. For the former one speaks of the fluctuations of the levels. Specifically one studies the statistical properties of the nearest neighbor spacing (NNS) distribution for adjacent states that have the same set of conserved quantum numbers. This method evaluates the fluctuations in level spacings, which get smoothed out as the system becomes chaotic. For the ordered systems, on the other hand, the levels are uncorrelated and thus have random energies, with exponentially decreasing number of level spacings as the spacing size increases. Thus for the ordered system, the NNS follows the Poisson distribution

$$P(s) = \exp(-s) \quad (1)$$

and for a generic chaotic system, the NNS follows the Wigner distribution [1]

$$P(s) = \pi/2s \exp(-\pi s^2/4), \quad (2)$$

where  $P(s)ds$  measures the probability of having levels with spacing in the interval between  $s$  and  $s+ds$ . Here  $s$  is a dimensionless parameter. It is measured in units of mean-level spacing.

The smoothing of the level spacing for a quantum system can be understood as level repulsion resulting from the mixing of states. Using the random matrix theory (RMT), which was initiated by Wigner [2] and extended by Dyson and Mehta [3,4], it has been shown that a Gaussian orthogonal ensemble (GOE) provides a complete description of quantum chaos in systems with time-reversal symmetry [1]. The mixing depends on the ratio  $v/d$ , where  $v$  is the average interaction potential between the levels and  $d$  is their average energy separation. The random matrix theory has been used to explain the rotational level statistics of compound-nuclei with good success [5,6].

Quantum chaos has been investigated in many different fields and in many simple model problems with two degrees of freedom. These model problems provide the simplicity in that actual numerical calculations can be carried out with good accuracy either classically or quantum mechanically. Quantum chaos has been studied in atomic physics in 1980's and 1990's. In particular, the spectra of a hydrogen atom in a magnetic field [7,8] and the spectra of helium atoms have been extensively studied both in theory and experiment. Despite these earlier efforts, evidence of quantum chaos in helium atom is still elusive.

In this paper, we revisit the signature of quantum chaos in helium atom. In helium, almost all the classical orbits are unstable. The energy levels of the helium atom, on the other hand, are considered to be very regular, or ordered. For the ground state and the singly excited states, their energy levels are well described by the quantum numbers from the shell model. At higher energies, the shell model description of the

\*Email address: [atle@phys.ksu.edu](mailto:atle@phys.ksu.edu)

doubly excited states of helium has been known to be inadequate since the 1960's [9]. However, subsequent theoretical studies of doubly excited states in the 1970's through 1990's have confirmed that the spectra of these low doubly excited states are also regular [10]. Only at the highest energies studied, i.e., doubly excited states lying below the  $N=9$  threshold of  $\text{He}^+$ ,  $I_9$ , there is some subtle indication of a transition towards quantum chaos [11]. In other words, experimental evidence shows the energy levels of the helium atom are ordered, spanning from the ground state to  $I_9$ , or from 79 to 0.67 eV below the double ionization threshold. If quantum chaos is to exist in helium, the search has to be made at energies much closer to the double ionization threshold.

Extensive studies of quantum chaos of helium have been carried out by Reinhardt and Blümel in the 1990's using the so-called stretched 1D model [12,13]. In this model, each electron is restricted to move along in one dimension, and to maintain on opposite sides of the nucleus. With such a model, calculation on the energy levels can be carried out to higher  $I_N$ . For levels from  $I_{11}$  to  $I_{15}$ , they have shown that there is an indication that the NNS begins to show a larger deviation from the Poisson distribution towards the Wigner distribution, in comparison with the NNS for levels at lower energies. No quantitative evaluation of how the NNS distribution evolves towards the quantum chaos limit was discussed. On the experimental side, photoabsorption spectra of He below  $I_9$  have been studied by Püttner *et al.* [11]. From the measured spectra, the authors claimed to have observed evidence of transition towards quantum chaos. Since Wigner distribution is a limit for fully chaotic system, it is desirable to have a quantitative indicator that measures the closeness of NNS to the Wigner distribution as the excitation energy is increased.

The NNS distributions have also been studied for the low-lying states in many-electron atoms with a few open shells by various authors [14–16]. In this case, the NNS has been found to be quite close to the Wigner distribution. These states have low excitation energies. Such core-induced quantum chaos has no classical analog and is considered to be different from the one studied here for helium. Such core-induced quantum chaos has also been studied in atoms, such as lithium, in a magnetic field [17]. The Wigner distribution of these levels is a consequence of spectral repulsion, and is considered to be different from quantum chaos where the classical motion is chaotic. To distinguish such core-induced chaos, other indicators beyond the NNS have been proposed [18,19].

The rest of this paper is arranged as follows. In the next section we first summarize the previous studies of the doubly excited states of He. We then summarize previous theoretical studies of the NNS distributions based on the one-dimensional model He atom and address the issues of resonance widths since most of the doubly excited states are autoionizing states. In Sec. III we first introduce the hyperspherical close-coupling method that was used to calculate the energy levels. We stress that the main breakthrough owes to the possibility of diabaticizing the adiabatic hyperspherical potential curves which in turn allows us to throw away potential curves that are considered to be irrelevant. The trun-

cation of the number of channels permits us to calculate helium spectra to much higher  $I_N$  than previously possible and to generate data at energies much closer to the double ionization threshold. We also discuss how to select levels for the NNS analysis. Rydberg levels that can be attributed to individual  $I_N$  are excluded. We adopted the so-called Brody parameter  $q$  to measure the transition from the Poisson distribution ( $q=0$ ) to the Wigner distribution ( $q=1$ ). Thus a Brody parameter  $q$  will be derived for each NNS distribution analyzed. To simplify the calculation and to extend to much higher  $I_N$ , we also used a so-called  $s$ -wave model to study level spacing statistics up to  $I_{30}$ . For this purpose potential curves up to  $I_{40}$  have been calculated in order to study the spectral interaction from these higher levels. The results of the calculations and the analysis are presented in Sec. IV. We also investigated the dependence of the NNS on the charge of the nucleus for a fixed scaled energy region, and also for different symmetries. Such dependence were studied using the  $s$ -wave model. For the real 3D helium, we calculated the NNS for  $^1S^e$  doubly excited states between  $I_{14}$  and  $I_{19}$ , and a Brody parameter  $q=0.66$  was found. This shows that the rate of reaching  $q=1$  for the Wigner distribution is rather slow. In the last section we summarize our results and discuss future studies, possibly in connection with the Wannier threshold law [20]. The physics of two electrons with total energy of only a few to tens of meV's above or below the full breakup threshold is in its own world. With the new theoretical tools developed in the present paper, we believe that future quantitative studies of helium in this narrow energy region are becoming possible. Atomic units are used throughout the paper unless otherwise stated.

## II. ENERGY LEVELS OF THE HELIUM ATOM

The energy eigenvalues of helium atom have been calculated since the birth of quantum mechanics. For the present purpose, we treat helium atom by a nonrelativistic Hamiltonian (with  $Z=2$ )

$$H = -\frac{1}{2}\nabla_1^2 - \frac{1}{2}\nabla_2^2 - \frac{Z}{r_1} - \frac{Z}{r_2} + \frac{1}{r_{12}}. \quad (3)$$

We do not include any spin or other relativistic interactions. Thus the eigenstates of the Hamiltonian are eigenfunctions of  $L^2$ ,  $S^2$ ,  $L_z$ ,  $S_z$ , where  $\mathbf{L}$  and  $\mathbf{S}$  are the orbital and spin angular momentum operators, respectively, with the quantization axis chosen along a space-fixed direction. The eigenstates of  $H$  also have well-defined parity  $\pi$ . The global symmetry of the helium eigenstates can thus be designated by  $^{2s+1}L^\pi$ .

### A. Lack of experimental evidence of quantum chaos in He

Within the shell model, each eigenstate is also designated by  $nl$  and  $Nl'$  quantum numbers from each electron, with  $n(N)$  the principal quantum number and  $l(l')$  the orbital angular momentum of each electron. We will choose the convention that  $n \geq N$ , such that  $N$  is the principal quantum number of the inner electron. With these conventions, we now discuss the spectrum of helium. The singly excited states

such as  $1sns\ ^1S^e$  or  $1snp\ ^1P^0$  have been well studied. The energy levels for each series follow the well ordered Rydberg formula. There is no chaos to talk about if only one electron gets excited.

As the excitation energy increases, resonances corresponding to doubly excited states emerge. Consider doubly excited states below  $I_2$  that were first measured by Madden and Codling in 1963 [21]. According to the shell model, three ordered Rydberg series  $2snp$ ,  $2pnd$ , and  $2pnd\ (^1P^0)$  are expected, each converging to the same  $I_2$ , if these series do not “interact.” However, theoretical calculations showed that they have strong configuration mixing [22]. The “interaction,” however, does not alter their regular ordered spectra. Instead three new “independent” Rydberg series emerge, which were called by Fano and co-workers [9] as  $+$ ,  $-$ , and  $pd$  series. Subsequent group-theoretical analysis [23] and hyperspherical approach [10,24] showed that these doubly excited states can be classified with a new set of approximate quantum numbers. Basically, the  $l$  and  $l'$  in the shell model are replaced by a new set of quantum numbers, while  $n$  and  $N$  can still be treated as good quantum numbers. Thus a doubly excited state can be labeled by  $(K, T)^A$  where  $A$  takes only  $+$ ,  $-$ , or  $0$ , in addition to  $N$  and  $n$  for each fixed  $L$ ,  $S$ , and  $\pi$  [24,10]. Using a hyperspherical approach, below each  $I_N$ , each channel (or series) is represented by a potential curve similar to the Born-Oppenheimer potential curve in molecules and the channel is labeled by  $(K, T)^A$ . For each potential curve, if the interaction with other curves is neglected, then the eigenvalues form an ordered spectrum. Thus if the coupling among these different hyperspherical channels is weak, the spectra of doubly excited states is a collection of ordered series. This is the case for all the doubly excited states below the  $I_5$  threshold [25].

The fact that the channels belonging to the same  $I_N$  only interact very weakly has been traced to the collective bending vibrational motion of the two electrons. In fact, one can replace  $K$  and  $T$  by a bending vibrational quantum number  $v = N - K - T - 1$  [10,26,27]. Thus the different Rydberg series below each  $I_N$  correspond to states of different vibrational modes. From the viewpoint of the shell model, doubly excited state have strong configuration mixing. But the mixing results in new ordered spectra. In other words, the interaction among the shell-model states does not give rise to spectral repulsion, and there is no quantum chaos in doubly excited states in helium from the interaction of levels within the same  $I_N$ . Experimental photoabsorption spectra below  $I_2$  through below  $I_4$  clearly show that the spectra are ordered [25].

As photoabsorption spectra were pushed to higher energies, local deviation from regularity begins to emerge. These local irregularities have been observed starting with resonances below  $I_5$  [25], where the intensity of several Rydberg resonances can undergo modulations. Such phenomena are well known in atomic physics and are often analyzed using the multichannel quantum defect theory [28]. In helium, the modulation is the result of a broad resonance interacting with several states of another Rydberg series in the same energy region. This broad resonance is the “intruder” from the lowest member of the Rydberg series converging to the next higher threshold. The intruder state in general has low prin-

cipal quantum number and lies closer to the nucleus. The higher members of the Rydberg series, on the other hand, have larger principal quantum numbers and are farther away from the nucleus. Even though these states overlap in energies, their interactions are weak, and the individual Rydberg series is still discernible, except modified by the modulation. These spectral features are known as overlapping resonances. As the excitation energy increases further, the number of intruder states increases. In the experiment of Püttner *et al.* [11] for resonances below  $I_9$ , intruders from  $N=10$  and  $11$  channels enter, and deviation from regularity starts to appear. In other words, we may say that glimpse of possible evidence of quantum chaos begins to emerge below  $I_9$ , but the spectra are still qualitatively similar to the spectra at lower energies. To see quantum chaos, spectra at higher energies would be needed. Unfortunately, spectra below  $I_9$  appear to be where the third-generation synchrotron radiation has reached its limit. Interestingly, this is also roughly the energy region where the theoretical method has reached its limitation at the time (2001) [11].

### B. Theoretical search of quantum chaos in He

In the past 40 years, many theoretical methods have been developed to calculate the energy levels (and their widths) of doubly excited states of helium, mostly based on the Hamiltonian given by Eq. (3). Very accurate results have been achieved from these calculations and good agreement with experimental measurements have been reported (see the review paper [29]). However, most of these calculations can be used to calculate doubly excited states up to  $I_8$  or  $I_9$  only, for example, Refs. [30–32]. In selective cases [33] where calculations have been carried out to higher  $N$ , only a limited number of states were calculated for each symmetry and the analysis of their level spacing statistics is not possible.

In Püttner *et al.* [11], doubly excited states below  $I_9$  have been calculated using a complex-rotation method [31]. Their calculation were carried out using a Cray98 supercomputer. While their results were shown to agree very well with the experimental photoabsorption spectra, the number of levels obtained was too small for level spacing analysis. As a result, they have to resort to study the model one-dimensional (1D) He, where the system has only two degrees of freedom. From the cumulative NNS, they showed that the energy levels statistics gradually approaches the Wigner distributions for levels from below  $I_9$  to below  $I_{17}$ . To improve the statistics, the levels in a given energy region were calculated for slightly different values of the nuclear charge  $Z$ , from  $1/Z=0.45$  to  $0.55$  in steps of  $0.01$ .

The level statistics of 1D helium atom has also been studied previously by Reinhardt and Blümel [12]. For such “stretched” 1D helium where the two electrons are on the opposite sides of the nucleus, many classical and semiclassical calculations have also been carried out. In their quantum calculations, they showed that for levels between  $I_1$  and  $I_5$ , the NNS distribution simply reflects regular sequences of states that converge to the excitation thresholds. For states between  $I_6$  and  $I_{10}$ , and then for levels between  $I_{11}$  and  $I_{15}$ , they saw increasingly that the distribution is moving toward

the Wigner type. They did not perform quantitative analysis of the deviation of NNS from the Wigner distribution.

### C. Resonance widths and Ericson fluctuation

Most of the doubly excited states of He, as well as of the model 1D He, are resonances where each resonance state has its own width. If the width is small compared to the level separation, asymmetric Fano profile can be observed or calculated for each individual resonance. This is the case for all doubly excited states below  $I_4$ . For doubly excited states above  $I_5$  through  $I_9$ , as indicated earlier, the so-called overlapping resonances appear because of the presence of intruder states from the higher channel(s). A limited number of intruder states can modify the spectra locally to produce local irregularity. For quantum chaos to appear, the number of intruder states needs to be large enough, and the interaction among them be strong, such that the level spacings become more evenly distributed. In this limit, evidence of quantum chaos will be seen experimentally with the appearance of Ericson fluctuation [34] in the photoabsorption spectra where the identity of each resonance is lost and the cross section would fluctuate strongly as a function of energy. No such evidence of Ericson fluctuations has ever been observed or predicted theoretically in atoms as yet except in model 1D He calculations [35].

## III. THEORETICAL METHODS

### A. Hyperspherical approach and partial diabatization

We chose to use scaled coordinates  $\mathbf{r} \rightarrow Z\mathbf{r}$  and scaled energy  $E \rightarrow E/Z^2$ , where  $Z$  is the charge of the nucleus. The Schrödinger equation for a two-electron atom with nuclear charge  $Z$  is then written as follows:

$$\left[ -\frac{1}{2}\nabla_1^2 - \frac{1}{2}\nabla_2^2 - \frac{1}{r_1} - \frac{1}{r_2} + \frac{1}{Zr_{12}} - E \right] \psi(\mathbf{r}_1, \mathbf{r}_2) = 0. \quad (4)$$

Here,  $\mathbf{r}_1$  and  $\mathbf{r}_2$  are the coordinates of the two electrons and  $r_{12}$  is the interelectronic distance. Using the scaled coordinates, the nonseparable interelectronic interaction term decreases with the nuclear charge. In the limit of  $Z \rightarrow \infty$ , the system is separable and the NNS is expected to follow Poisson distribution.

We solved the Schrödinger equation (4) by using hyperspherical coordinates within the general framework of the hyperspherical close-coupling (HSCC) method [30,36,37]. Starting with the radius vectors of the two electrons  $\mathbf{r}_i = r_i \hat{\mathbf{r}}_i$ , the hyperradius  $R$  and hyperangle  $\alpha$  are defined as

$$R = \sqrt{r_1^2 + r_2^2}, \quad (5)$$

$$\tan \alpha = \frac{r_2}{r_1}. \quad (6)$$

In this coordinate system, the rescaled wave function  $\Psi = \psi R^{3/2} \sin \alpha \cos \alpha$ , satisfies

$$\left( -\frac{1}{2} \frac{\partial}{\partial R} R^2 \frac{\partial}{\partial R} + \frac{15}{8} + H_{\text{ad}}(R, \Omega) - R^2 E \right) \Psi(R, \Omega) = 0, \quad (7)$$

where  $\Omega \equiv \{\alpha, \hat{\mathbf{r}}_1, \hat{\mathbf{r}}_2\}$ .  $H_{\text{ad}}$  is the adiabatic Hamiltonian with the hyperradius fixed

$$H_{\text{ad}}(R, \Omega) = \frac{\Lambda^2}{2} + RC(\Omega). \quad (8)$$

Here  $\Lambda^2$  is the square of the grand-angular momentum operator and  $C(\Omega)$  is the effective charge,

$$C(\Omega) = -\frac{1}{\sin \alpha} - \frac{1}{\cos \alpha} + \frac{1}{Z\sqrt{1 - \sin 2\alpha \cos \theta_{12}}}, \quad (9)$$

where  $\theta_{12}$  is the angle between  $\mathbf{r}_1$  and  $\mathbf{r}_2$ .

In the adiabatic approach, the adiabatic channel functions are defined as the eigenfunctions of  $H_{\text{ad}}$  with the adiabatic potential energies  $U_\mu(R)$ . We solve this eigenvalue problem for each fixed  $R$  using partial-wave expansion in  $\{\hat{\mathbf{r}}_1, \hat{\mathbf{r}}_2\}$ , including up to 26 partial waves. For the hyperangle  $\alpha$  we employ the discrete variable representation (DVR) [38] based on the Gauss-Jacobi quadrature with about 900 DVR points. The total wave function is then expanded in the adiabatic basis set, which results in the coupled-channel equations for the hyperradial components.

In practical numerical calculations, adiabatic basis functions are no longer directly used to obtain the coupled differential equations for the hyperradial components of the wave function because of the presence of numerous avoided crossings. Earlier HSCC calculations employed the so-called diabatic-by-sector method [30,36]. Lately the smooth variable discretization (SVD) technique developed by Tolstikhin *et al.* [39] was employed in the recent HSCC calculations. Both methods avoid the direct calculations and use of nonadiabatic coupling terms. The diabatic-by-sector method, in which each basis function is fixed within each sector, suffers from slow convergence and thus more basis functions are needed [40]. The SVD method only requires that the total wavefunction be smooth in the adiabatic parameter  $R$ . By expanding the hyperradial wavefunctions using DVR basis functions, a new set of hyperangular basis functions are obtained and they are used together to propagate the total wave function from one end of the sector to the other end. This method is very efficient and accurate and has been used in many ‘‘contemporary’’ HSCC calculations [37,41–46].

The SVD method as used in the HSCC calculations is highly algebraic. It fully eliminates the direct reference to potential curves and their avoided crossings. Still these potential curves and avoided crossings offer good starting point for understanding the basic dynamics of each problem. In the recent applications of HSCC to ion-atom collisions at low energies, we have developed another modification to the SVD method. The main idea is to transform all the sharp avoided crossings into real crossings, but without actually calculating the nonadiabatic couplings directly. Our procedure differs from the full diabatization within a given set of adiabatic basis set used earlier by Heil *et al.* [47]. We diabatize a subset of adiabatic curves only when the overlap integrals are larger than a prescribed number. The procedure is

described elsewhere [48,49]. The effect is that all the sharp avoided crossings are transformed into real crossings. The broad avoided crossings would still remain avoided crossings. In this partial diabaticization method, no further approximation was made if all the coupling terms and all the channels are retained in the subsequent solution of the hyperradial equations.

In this new picture the potential curves and channel functions evolve smoothly with  $R$ . The most important advantage of such a procedure is that it allows us to remove unimportant potential curves or “channels” from the subsequent HSCC calculations. This method has been employed in a number of ion-atom and other collision systems [48–50] where we have been able to reduce the number of channels by a factor of 2 or 3, depending on the collision systems and collision energies. Since in general only 10–30 adiabatic channels are used in low-energy ion-atom collisions, such reductions do not save the computational time significantly, except that the dynamics becomes much more transparent in the reduced calculations.

In this paper, we will show that the elimination of channels can be used to drastically reduce the number of channels in problems associated with high-lying doubly excited states. For all the  $1S^e$  doubly excited states of He below  $I_{30}$ , for example, there are more than 500 channels. We can reduce the calculations to only about 30 channels, i.e., by keeping about less than 10% of the channels in the calculation. The elimination is possible since channels converging to the same  $I_N$  limit interact very weakly. Thus we include only the interaction for channels dissociating to different thresholds, i.e., channels that generate the intruder states. Examples of such elimination will be shown later.

### B. Level spacings analysis

Suppose we have a sequence of energy levels  $E_1 \leq E_2 \leq \dots \leq E_n$ . The integrated (or cumulative) level density is defined as follows:

$$N(E) = \sum_{i=1}^n \Theta(E - E_i), \quad (10)$$

where  $\Theta(E)$  is the Heaviside step function. Function  $N(E)$  can be decomposed into two parts, a smooth average part and a fluctuating part

$$N(E) = N_{\text{av}}(E) + N_{\text{fl}}(E). \quad (11)$$

The fluctuation part is used to compare different systems which may have different average behavior. Therefore, in practice one performs the unfolding procedure to get rid of the average smooth part. Technically speaking, one performs a mapping from the old variables  $E_i$  to new variables  $\epsilon_i$ ,  $E_i \rightarrow \epsilon_i$ , with  $\epsilon_i = N_{\text{av}}(E_i)$ . In other words, in the new variables, the integrated level density is a straight line and the mean spacing is a constant, scaled to unity.

Clearly, the unfolding procedure is by no means unique as it depends on the way the decomposition (11) is performed. In this paper we follow the unfolding procedure given in Refs. [51,52]. First, the local mean spacing  $D_i$  for each spac-

ing  $\sigma_i = E_{i+1} - E_i$  is obtained by averaging over an equal number of neighboring spacings on either side of  $E_i$ ,

$$D_i = \frac{1}{2k+1} \sum_{j=-k}^k \sigma_{i+j}. \quad (12)$$

The new spacing  $s_i = \epsilon_{i+1} - \epsilon_i$  is then defined as

$$s_j = \sigma_i / D_i. \quad (13)$$

In other words, one performs the mapping

$$\epsilon_{i+1} = \epsilon_i + (2k+1) \frac{E_{i+1} - E_i}{E_{j_2+1} - E_{j_1}}, \quad (14)$$

where  $j_1 = \max(1, i-k)$  and  $j_2 = \min(n-1, i+k)$ . The statistical measures depend on the number of included consecutive spacings  $k$ , which are used to calculate the local mean spacing in Eq. (12). Therefore we require stability with respect to small changes in  $k$ . Typically we use  $k=5$  up to  $k=10$ . Finally, to make sure of the stability with respect to unfolding procedure we also unfold our spectra by fitting the smooth part of the integrated level density by a polynomial expansion

$$N_{\text{av}}(E) = \sum_{i=0}^m a_i E^i, \quad (15)$$

and, subsequently, a mapping  $E_i \rightarrow \epsilon_i$ , with  $\epsilon_i = N_{\text{av}}(E_i)$ .

Having unfolded the energy spectrum, we can now calculate the NNS distribution  $P(s)$  which is the distribution of the variable  $s_i = \epsilon_{i+1} - \epsilon_i$  and compare it with the Poisson and Wigner distributions. To have an idea how the distribution is close to the Poisson or Wigner distributions it is convenient to fit  $P(s)$  to the Brody distribution [53]

$$P_q(s) = \alpha s^q \exp(-\beta s^{q+1}), \quad (16)$$

with

$$\alpha = (1+q)\beta, \quad \beta = \left[ \Gamma\left(\frac{2+q}{1+q}\right) \right]^{1+q}. \quad (17)$$

The Brody parameter  $q$  varies from 0 for a Poisson distribution to 1 for a Wigner distribution and is a measure (but not the only one) of the level repulsion.

## IV. RESULTS AND DISCUSSIONS

### A. Diabatic potential curves

To illustrate the numerical procedure used for this work, in Fig. 1 we show all the seven  $1P^0$  potential curves converging to  $I_4$ , plus another curve converging to  $I_5$ . The original adiabatic potential curves are shown in dashed lines while the solid lines are the diabatic curves. Note that they differ mostly only in the region of sharp avoided crossings. In Fig. 1 most of the crossings involve only two curves, but in one case the crossings involve three nearby curves. This figure illustrates that the diabaticization procedure does work well.

The diabaticized potential curves within each manifold that go to the same  $I_N$  limit can be designated by the set of

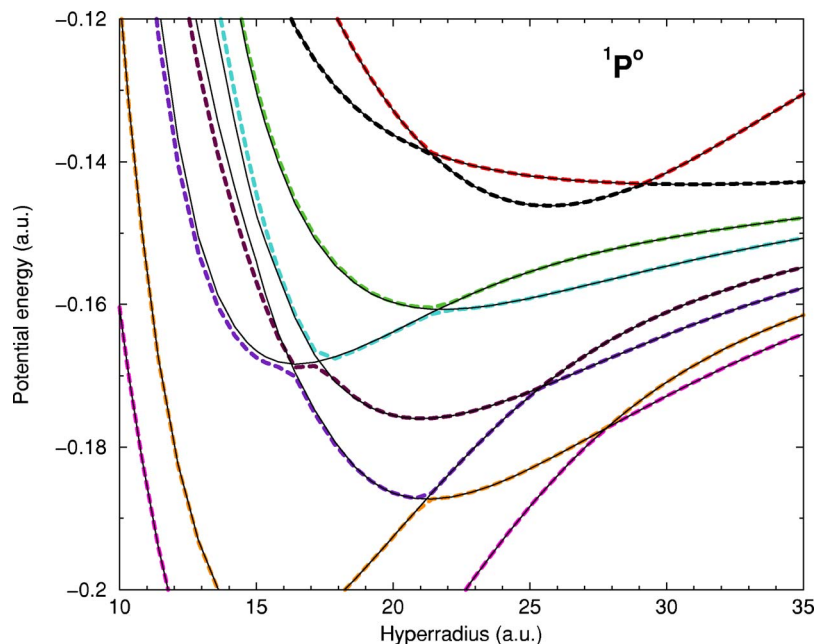


FIG. 1. (Color online.)  $\text{He}(^1P^0)$  potential curves converging to  $I_4$  and the lowest curve converging to  $I_5$ . The thick colored curves are adiabatic, the thin black curves are diabatic.

$(K, T)^A$  quantum numbers, one set for each channel. This designation implies that the coupling among the channels is weak. For low-lying doubly excited states, it has been shown that a single-channel approximation can adequately predict the binding energies of these doubly excited states [54–56].

We next show the high-lying  $^1S^e$  potential curves of He, for channels between  $I_{12}$  and  $I_{24}$ , in Fig. 2. The initial adiabatic potential curves have been diabaticized. The lowest curve below each  $I_N$  has been marked in thick red lines. By selecting only the lowest curve from each  $I_N$  manifold, we regroup all these diabatic potential curves in Fig. 3. In this figure, the horizontal scale is given by  $\sqrt{R}$ . The potential curve at each point is expressed in terms of the effective principal quantum number  $N_{\text{eff}}(R) = \sqrt{-2/U(R)}$ , such that in the asymptotic limit, the vertical scale measures the principal quantum number  $N$  of the  $I_N$  threshold. It is clearly seen that strong

avoided crossings appear between successive curves.

We comment that for  $^1S^e$  symmetry, there are  $N$  channels converging to each threshold  $I_N$ . Each of these channels can be designated by  $(K, T)^A = (K, 0)^+$ , with  $K = N-1, N-3, N-5, \dots, -(N-1)$ . The lowest curve within each manifold has  $K = N-1$  for the  $^1S^e$  symmetry. One can define a bending vibrational quantum number  $\nu = N - K - T - 1$  such that all the potential curves in Fig. 3 have  $\nu = 0$ , i.e., each corresponds to the ground state of the bending vibrational mode of the states associated with  $I_N$ . For these  $\nu = 0$  states, the two electrons tend to stay on opposite sides of the nucleus, similar to a stretched one-dimensional He atom.

In Fig. 3 we draw a dotted horizontal red line for each of the principal quantum numbers  $N = 3, 9$ , and  $18$ . Each is the limit for the Rydberg series associated with the respective  $I_N$ . As  $N$  increases, the number of potential curves from the up-

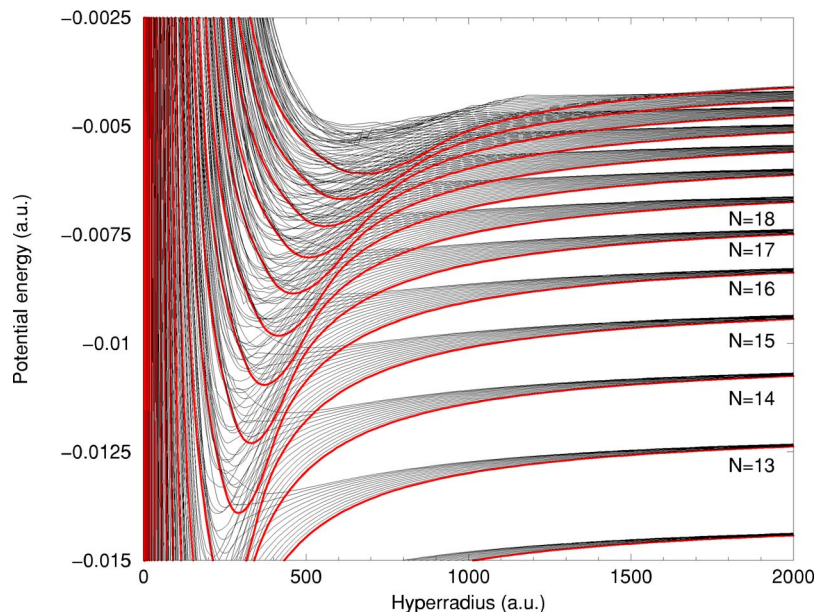


FIG. 2. (Color online.)  $^1S^e$  diabaticized potential curves for 3D helium between  $I_{12}$  and  $I_{24}$  ionization thresholds. The thick red curves correspond to the lowest curves from each manifold. They have the approximate quantum numbers  $K = N - 1$ .

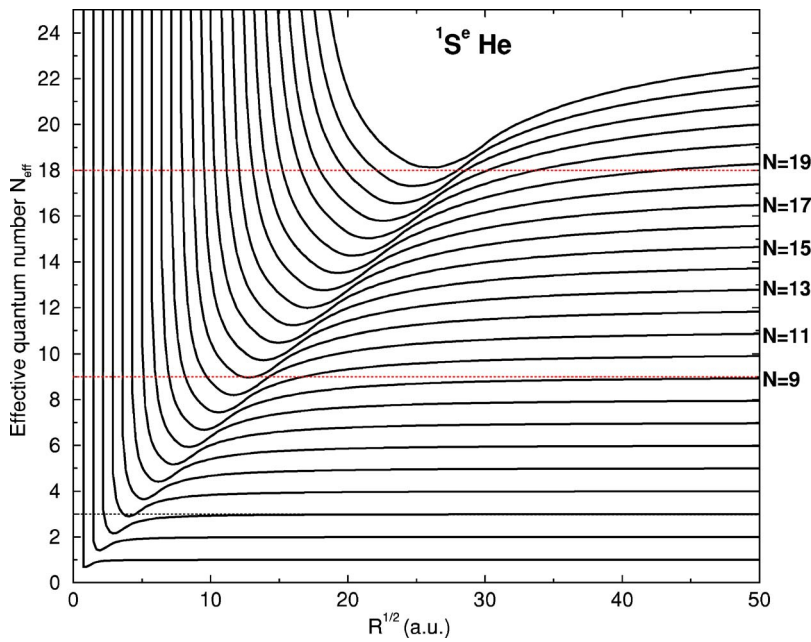


FIG. 3. (Color online.) Lowest potential curves from each manifold up to  $N=24$  for  $1S^e$  3D helium (that is, the red curves in Fig. 2), plotted as effective quantum numbers  $N_{\text{eff}}(R) = \sqrt{-2/U(R)}$  vs  $R^{1/2}$ .

per channels crossing the horizontal line increases. To illustrate this fact more clearly, we redraw these potential curves and show them against the hyperradius  $R$  in Fig. 4 for the three cases  $N=3$ , 9, and 18. For  $N=3$ , we note that the lower part of the  $N=4$  curve has actually penetrated below the  $I_3$  threshold, but the penetration is weak so that all the “bound” states from the  $N=4$  curve are above the  $I_3$  threshold. In this case the levels below  $I_3$  form a regular Rydberg series. For  $N=9$ , we note that the curves from  $N=10$  and 11 enter below  $I_9$ . The interaction of these channels results in overlapping

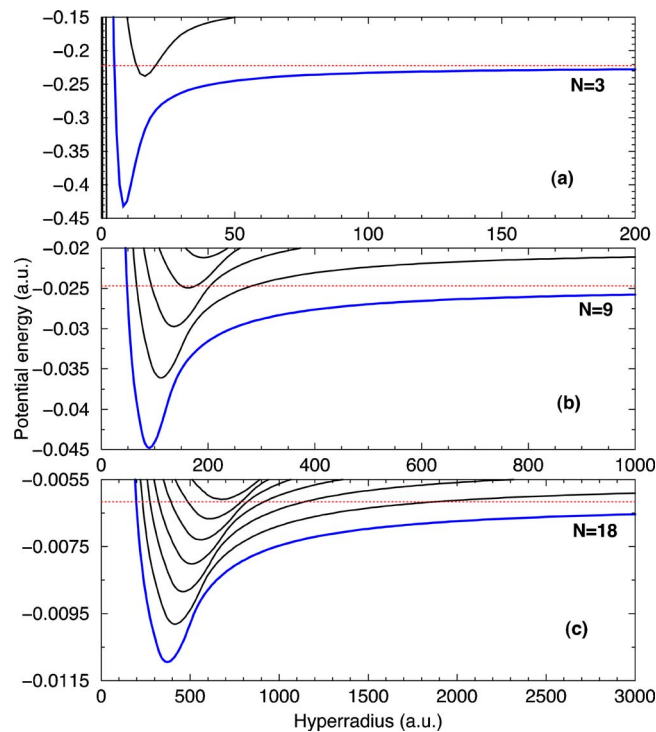


FIG. 4. (Color online.) Close-up of the  $1S^e$  hyperspherical potential curves in the energy region near the  $I_3$ ,  $I_9$ , and  $I_{18}$  thresholds.

resonances similar to those observed in Püttner *et al.* [11].

The situation for  $N=18$  is different where the potential curves from many more channels,  $N=19-23$ , penetrate below  $I_{18}$ . If these channels do not interact, the energy levels supported by each potential curve can be calculated. The results from such calculations are shown in Fig. 5, labeled under columns (a)–(e), for  $N=18$  to  $N=22$ , respectively. For  $N=23$ , there is no “bound” state in the energy range shown in Fig. 5. Grouping all these “noninteracting” levels together, the spectrum is shown under column (f). By including the couplings among these potential curves, new eigenvalues are obtained. The resulting energy levels are shown under column (g).

Comparing visually the levels under columns (f) and (g) in Fig. 5, it does appear that the levels in column (g) are

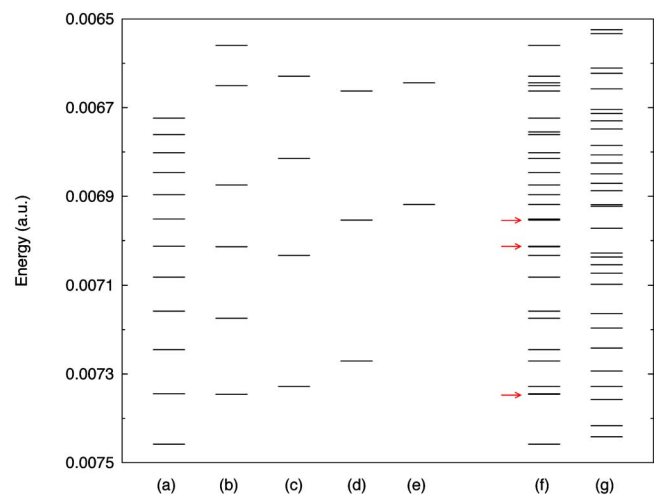


FIG. 5. (Color online.)  $1S^e$  energy levels below  $I_{18}$  threshold from one-channel calculations for  $N=18$  to  $N=22$ , in columns (a)–(e), respectively. Column (f) groups all “noninteracting” levels from (a)–(e) together and column (g) represents the results from coupled-channel calculations.

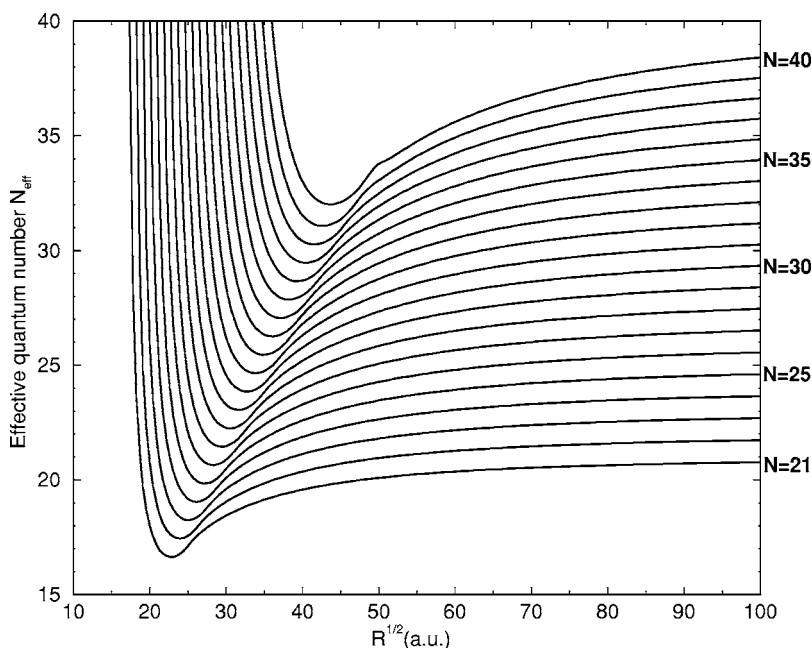


FIG. 6.  $^1S^e$  potential curves for  $s$ -wave model of helium ( $Z=2$ ) from  $N=21$  up to  $N=40$ .

more evenly separated. This is the consequence of spectral repulsion. For column (f), we use arrows to indicate places where two levels have very small level spacing. The existence of more abundant small level spacings is characteristic of Poisson distribution. In such a small sample and limited calculation, we do still get one pair of levels in column (g) where the level spacing is small. We definitely have observed spectral repulsion, but the NNS as shown below, definitely is not reaching near the Wigner distribution yet. To reach that limit, levels at higher  $N$ 's are needed. In the meanwhile, we comment that higher Rydberg states belonging to  $N=18$  have been removed from the NNS analysis, following the prescription of Eq. (18) below.

### B. The $s$ -wave model of He

In the so-called  $s$ -wave model, we limit the orbital angular momentum of each electron to zero, thus for each  $I_N$  threshold, there is only one channel. This model has been used previously in the literature [57,58]. Using this model, we can easily extend our calculations to much higher thresholds. For the present purpose, it is adequate that we limit our calculations to potential curves below  $I_{40}$ . The energy levels will be calculated and the level spacing statistics will be examined.

The singlet potential curves from  $N=21$  up to  $N=40$ , expressed in terms of effective quantum numbers  $N_{\text{eff}}(R) = \sqrt{-2/U(R)}$  for  $Z=2$ , are presented in Fig. 6. The pronounced avoided crossings in the potential curves are clearly seen. These avoided crossings are known to be crucial in understanding the dynamics of this model problem. Furthermore, the number of “intruding” channels becomes larger as energy (or effective quantum number) increases. For  $N=21$ , there are 6, and for  $N=30$ , there are 8. First we will examine the level spacing statistics vs the nuclear charge  $Z$ .

Before we proceed further, it is important to clarify the ways how the data were calculated and how they are sampled. First, except for  $Z=\infty$ , the calculated doubly ex-

cited states (i.e., states which lie above  $I_1$ ) are resonance states. Each state has a position and a width. In our calculation, we treat each as a bound state. Second, below each ionization threshold, there always exists a certain range of energy where energy levels are regular (the so-called Rydberg regime). These levels should be excluded from the statistical analysis. If these Rydberg levels are also included in the level statistics analysis, then for Coulomb systems pure Wigner distribution could never be reached. Such example has been studied by Zakrzewski *et al.* [59] for the energy levels of hydrogen atom in a magnetic field.

In our procedure, first we solve the hyperradial coupled equations to obtain the discrete eigenfunctions using the DVR basis set associated with Laguerre polynomials  $\{L_n^{(3)}\}$ , which exponentially decline for  $R \rightarrow \infty$ . To obtain eigenvalues between  $I_{25}$  and  $I_{30}$ , for example, we chose the maximum value of the quadrature abscissas  $R_{\text{max}}=15\,000$  and channels below  $I_{25}$  were excluded in the coupled equations. To exclude Rydberg states close to each threshold and possible pseudostates from the calculated eigenvalues, we make sure that the states included in the analysis are all confined within a smaller box of  $R_{\text{box}} < R_{\text{max}}$ . Thus the states should satisfy the condition

$$\int_0^{R_{\text{box}}} |\Psi(R)|^2 dR \geq \varepsilon, \quad (18)$$

where  $\varepsilon$  is typically chosen to be 0.85 and  $R_{\text{box}}/R_{\text{max}} \approx 2/3$ .

We chose  $Z=2, 6$  and infinity. Clearly when the nuclear charge reaches infinity, the interaction between the two electrons can be neglected and the Hamiltonian is separable. The scaled energy levels are given by  $E(n, N) = -1/(2n^2) - 1/(2N^2)$ . While the energy levels from each electron follow the simple regular hydrogenic expression, the level spacing statistics for this noninteracting overlapping system is the Poisson distribution. Although the energy levels for the independent-electron case are known analytically, we have

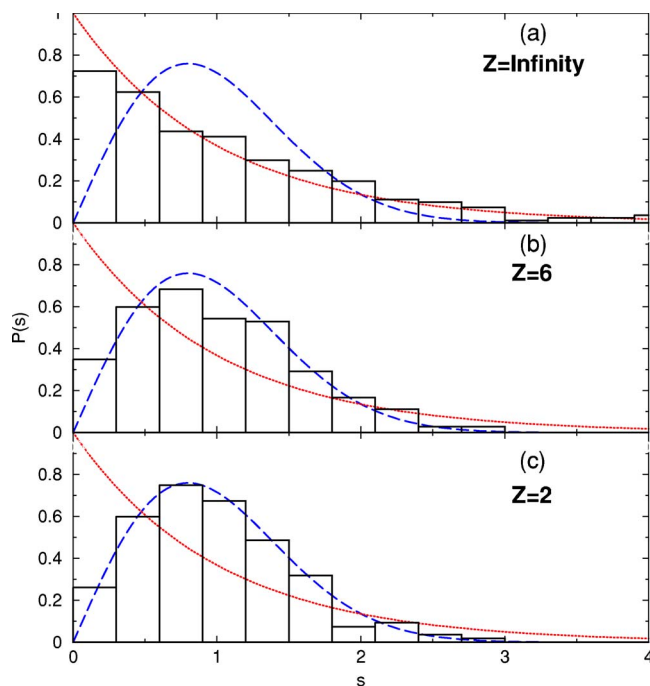


FIG. 7. (Color online.) NNS distribution from HSCC calculations in the energy range  $I_{25} < E < I_{30}$  for an  $s$ -wave  $1S^e$  model two-electron atoms with nuclear charges  $Z = \infty$  (i.e., independent electrons) (a),  $Z = 6$  (b), and  $Z = 2$  (c). The Poisson and Wigner distributions are shown as the dotted red and dashed blue curves, respectively.

calculated them using HSCC so we can compare the three cases on equal footing.

Our results are presented in Figs. 7(a)–7(c) for  $Z = \infty$ , 6, and 2, respectively, in the energy range  $I_{25} < E < I_{30}$ . Figure 7(a) shows that the NNS distribution for  $Z = \infty$  does indeed match the Poisson distribution quite well. The results for  $C^{4+}$

in Fig. 7(b) show closer to the Wigner distribution. The NNS distribution for the case of helium, shown in Fig. 7(c), is already quite close to the Wigner distribution. There are 283, 253, and 180 levels included in the statistical analysis for  $Z = \infty$ , 6, and 2, respectively.  $R_{\max} = 15\,000$  and  $R_{\text{box}} = 10\,000$  were used for all three cases.

The closeness to the Poisson or Wigner distributions can be measured in terms of the Brody parameter  $q$ . Recall that Brody parameter is zero for Poisson distribution and 1 for Wigner distribution. For  $Z = 6$ , we obtained  $q = 0.73$  and for  $Z = 2$ ,  $q = 0.95$  in the energy range  $I_{25} < E < I_{30}$ . Thus for the  $s$ -wave model of He, the NNS distribution is quite close to the Wigner distribution for this energy range. Note that the Brody parameter is simply one of the methods to measure the degree towards quantum chaos. Or more precisely, a measure of the degree towards the Wigner distribution. The actual number has no real significance but the trend clearly points out that the level spacing is closer to the Wigner distribution for helium than for  $C^{4+}$  in the same range of scaled energy. This is consistent with our expectation that the inter-electronic term which is responsible for the chaos is reduced for higher nuclear charge  $Z$ .

### C. Level spacing statistics of 3D He between $I_{14}$ and $I_{19}$

We now analyze the level spacing statistics of He where the energy levels are calculated from the diabaticized potential curves shown in Fig. 3. Following the method presented in the previous subsection for the  $s$ -wave model, we have analyzed the levels with energies between  $I_{14}$  and  $I_{19}$ . There were 139 levels used in the analysis and  $R_{\max}$  and  $R_{\text{box}}$  were 3000 and 2000, respectively. In Fig. 8 the NNS distribution obtained from such a calculation is shown. The Brody parameter calculated from the distribution was  $q = 0.66$ . This is still quite far away from  $q = 1.0$  for the Wigner distribution. It is in principle possible to extend our calculations to probe

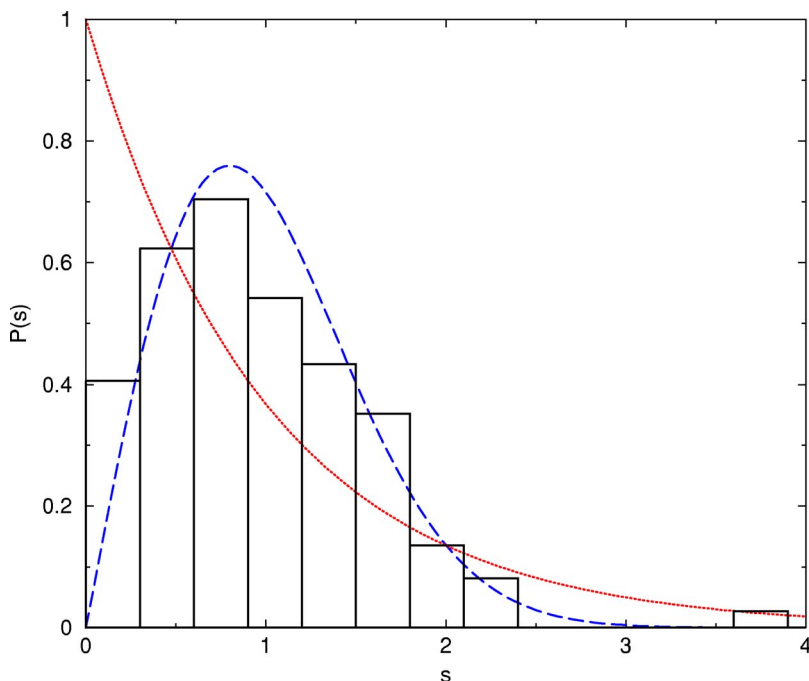


FIG. 8. (Color online.) NNS distribution for  $1S^e$  states from real 3D HSCC calculations for the energy range  $I_{14} < E < I_{19}$ . The Poisson and Wigner distributions are shown as the dotted red and dashed blue curves, respectively.

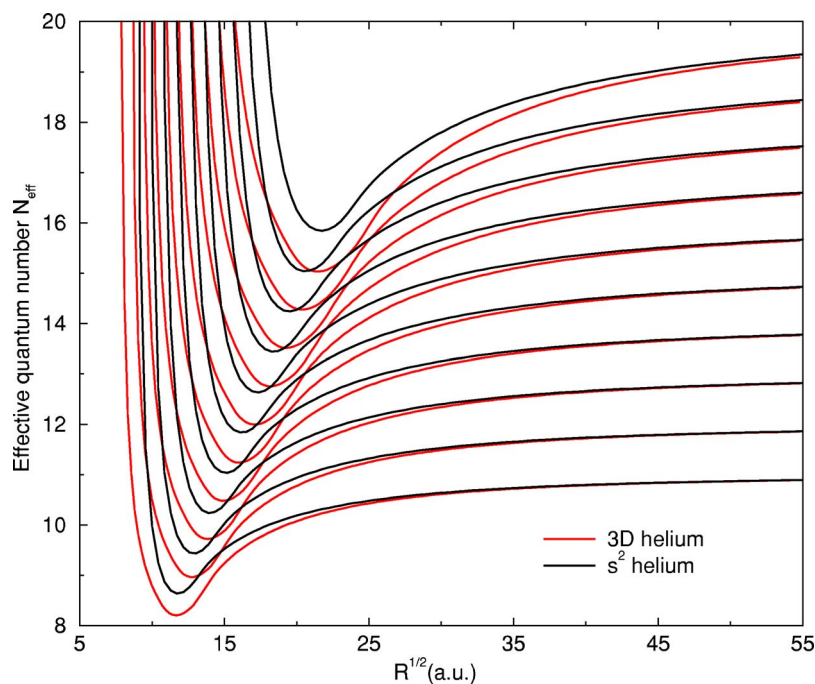


FIG. 9. (Color online.) Comparison between the  $1S^e$  potential curves from  $N=11$  to  $N=20$  for the  $s$ -wave model of helium and  $K=N-1$  potential curves of real 3D helium.

the NNS for levels of much higher  $I_N$  where a greater Brody parameter  $q$  is expected. However, the effort is probably not justified since the trend has been shown in the  $s$ -wave model already (see also Püttner *et al.* [11] and Blümel and Reinhardt [12] for the trend in the 1D stretch helium model). Instead, we compare the present true 3D calculations with the  $s$ -wave model for the same energy range of  $I_{14}$  to  $I_{19}$ .

In Fig. 9 the lowest potential curves from each manifold of 3D helium are compared to the potential curves from the  $s$ -wave model for  $N=11$  up to  $N=20$ . Note that their asymptotic thresholds are identical. For each threshold, the potential well from the 3D calculation is deeper than its corresponding one in the  $s$ -wave model. This is easily understood since in the 3D calculation, for the channels selected the two electrons tend to stay on opposite sides of the nucleus such that they have less interelectronic repulsion. A closer inspection also shows that the strength of the avoided crossing (narrower gap) between successive curves in the 3D model is stronger. Thus one expects that the spectral repulsion is stronger for the 3D system than for the  $s$ -wave model of He. We have examined the NNS for the  $s$ -wave model within the same  $I_{14}$  to  $I_{19}$  region and obtained a Brody parameter  $q=0.33$ . This shows that the  $s$ -wave model within the same energy region is further away from the chaotic region as compared to the real 3D helium in the same energy range, just as expected from our analysis. We note, however, that as the number of levels used in the analysis is quite small, the statistics is not so good in this case, which is also evidenced by quite a large  $\chi^2$  value for the fitting to the Brody distribution.

#### D. NNS distributions for triplet-S states

We next study how the different symmetry affects the NNS distributions. For this purpose, we employed only the  $s$ -wave model where the angular momentum of each electron

is again set to zero. However, by choosing the triplet symmetry, the spatial wavefunction changes sign under the exchange of two electrons. We analyze the same  $I_{25}$  to  $I_{30}$  region. For  $Z=2$ , we obtain  $q=0.80$ , to be compared to  $q=0.95$  for the singlet. For  $Z=6$ , we obtained  $q=0.46$  for the triplet, to be compared to  $q=0.73$  for the singlet. For  $Z$  goes to infinity, of course, the NNS is expected to be the Poisson distribution.

We thus easily conclude that the NNS distributions depend on the symmetry of the quantum system. For the triplet- $S$  symmetry of the  $s$ -wave model of He, the spatial wavefunction vanishes when the two electrons are at the same distance from the nucleus. Thus the effective interelectronic interaction is weaker and the avoided crossings between successive potential curves are weaker (not shown). The weaker spectral repulsion is reflected by their resulting NNS further away from the Wigner distribution as compared to singlet states in the same energy regime.

Although the above analysis was carried out for the  $s$ -wave model, we expect that qualitatively the conclusion applies to the real 3D system. The rate for approaching the Wigner distribution is faster for the  $1S^e$  states than for the  $3S^e$  states.

#### E. Generalization to other symmetries in He and other atomic and molecular systems

Based on our limited NNS distribution analysis for energy levels it is interesting to raise additional questions on a wide range of atomic systems where statistical analysis of the energy levels is more appropriate than the energies of individual states.

(1) First, the analysis can be extended to different symmetries of He. Examples of potential curves for  $1P^0$  have been shown in Fig. 1 where the seven curves below  $I_4$  and the lowest curve below  $I_5$  are displayed. Within the  $N=4$

manifold, the potential curves have been diabaticized and each curve can be labeled by the  $(K, T)^A$  quantum numbers. The  $v=0$  curves that are equivalent to what were used for the  $^1S^e$  states in Fig. 3 have  $K=N-2$ ,  $T=1$ , and  $A=+$ . Doubly excited states associated with this group of potential curves are prominently populated in photoabsorption of He from the ground state. The highest experimentally observed doubly excited  $^1P^0$  states are those below  $I_0$  measured by Püttner *et al.* [11]. No quantum chaos has been clearly seen in the experiment so far. The Brody parameter for this group of doubly excited states can be analyzed in the same way as for the  $^1S^e$  states.

(2) We anticipate the NNS distribution to approach the Wigner distribution as the excitation energy becomes close to the double ionization threshold for any symmetry or any finite nuclear charge in a two-electron atom or ion. In other words, the Brody parameter  $q$  will reach 1.0 as the double ionization threshold is approached. The key difference is the rate at which  $q$  approaches 1.0. Or alternatively, the difference is the value of  $q$  for a given range of excitation energies. We have seen such difference in the  $s$ -wave model for different  $Z$ , and between  $^1S^e$  and  $^3S^e$  states. For other symmetries, for example, for  $^1P^0$ , the curves from each  $I_N$  with  $K=N-1$ ,  $T=0$ , and  $A=-$  can couple with each other among the different  $N$ 's when  $N$  is large. These states also have  $v=0$  but the fact that they have  $A=-$  makes these states behave closer to the  $^3S^e$  states. Such analogy has been well studied for the low- $N$  doubly excited states. Their rate for approaching the Wigner distribution is expected to be as slow as the  $^3S^e$  states.

(3) Theoretical studies of classical and quantum chaos for the motion of three charged particles are often confined to He atom only. Nevertheless, one can ask about quantum chaos for other familiar systems involving three charged particles, such as  $H^-$ ,  $H_2^+$ , and  $e^+e^-e^-$ . For  $H^-$ , the present approach can be used directly for the NNS analysis. Without the actual calculation, we suspect that the Brody parameter  $q$  will be larger compared to He in the same scaled energy region. For  $H_2^+$ , within the same scaled energy region, we anticipate the Brody parameter to be smaller. Recall that within the Born-Oppenheimer approximation, the Hamiltonian for  $H_2^+$  is separable and the nonadiabatic coupling among the potential curve is very weak. Using mass-scaled hyperspherical coordinates [36,60], all of these systems can be studied on equal footing and the nonadiabatic coupling in  $H_2^+$  is weaker than in  $e^+e^-e^-$ , which in turn is weaker than in  $H^-$ . We thus expect the Brody parameter  $q$  be smallest for  $H_2^+$ , and highest for  $H^-$  in the same scaled energy region. In other words,  $H_2^+$  would have the slowest rate of approaching the Wigner distribution.

## V. SUMMARY AND CONCLUSIONS

In this paper we studied the signature of quantum chaos in helium atom by examining the nearest-neighbor spacing (NNS) distributions of the energy levels of doubly excited states which lie very close to the double ionization threshold. Specifically we calculated the energy levels of  $^1S^e$  states that lie between the  $N=14$  and 19 thresholds of  $He^+$  ion. These levels are only about 0.278 to 0.151 eV below the double

ionization threshold. Using the Brody parameter to quantify the degree of chaos, we found that  $q=0.66$  for the NNS distribution for these states. To examine the approach to the Wigner distribution in the chaotic limit, we also used the so-called  $s$ -wave model where the orbital angular momentum of each electron was restricted to zero. Using this model, we have analyzed the NNS distribution for the model He atom for levels between  $N=25$  and 30 thresholds of  $He^+$ . In this case we found  $q=0.95$  for He, indicating that at such high  $N$ , the Wigner distribution limit is almost reached. Existing experimental measurements and other theoretical calculations have been limited to levels below  $N=9$ . At such low  $N$ , there is limited signature of quantum chaos. We have also examined the NNS within the  $s$ -wave model for different nuclear charges, and for different symmetries. For levels that do not "interact" strongly, the Brody parameter in general would be smaller and significant signature of quantum chaos would occur at energies much closer to the double ionization threshold.

The solution of the Hamiltonian for the helium atom near the double ionization threshold in general is very complicated, with huge number of eigenstates within a small energy range. If all the levels within the given energy range are analyzed, the NNS would be Poisson distribution [11]. To see quantum chaos we need to be able to isolate levels that interact strongly. This is conveniently performed within the framework of the hyperspherical close-coupling method. With the implementation of the recently developed procedure for obtaining diabatic potential curves, it has been shown that potential curves that converge to the same  $I_N$  in general interact weakly, and each channel in the  $N$ th manifold can still be labeled by the set of  $(K, T)^A$  quantum numbers, or approximately speaking, by a unique vibrational quantum number  $v=N-K-T-1$ . By limiting only the interactions of the  $v=0$  channel from each threshold, we have drastically simplified the coupled channel calculations. The removal of most of the curves in Fig. 2 to end up with a very small set of curves in Fig. 3 exemplifies the major computational advance made in the present paper. We were able to carry out all the results reported in this paper on simple desktop personal computers.

While we have studied the NNS distribution, and used the Brody parameter to quantify the degree of approaching the Wigner distribution as a measure of quantum chaos, we caution that such a procedure is not unique. Since the classical helium atom is intrinsically chaotic at all energies [61], our measure of quantum chaos has been based on the NNS distribution alone. Alternative methods of parametrizing these level spacings may draw a somewhat different quantitative conclusion. However, the Brody parameter does provide a measure of the trend of NNS distribution towards the Wigner distribution for each system as the excitation energies are increased.

Another warning about the NNS distribution studied in this paper is in order. We have shown that the stronger interaction between nearby levels is needed to achieve a larger Brody parameter  $q$  towards 1.0, but such coupling, in real physical systems, would mean larger decay widths. Therefore these states have short lifetimes. Since classical chaos is a long-time phenomenon, the quantum chaos, as measured

using the NNS distribution, probably does not have direct bearing to the classical chaos. From the experimental point of view, the lifetimes of these levels are likely larger than the level spacings, such that the physical observable that would signify quantum chaos would be the Ericson fluctuations. Such phenomena have been observed in nuclear physics [62,63], but no such evidence has been found in atomic physics. The fact that they would occur at such a high energy near the double ionization threshold, as predicted by the present paper, explains why they are so elusive in atomic systems. The best chance where Ericson fluctuations can be observed in atoms would be in the photoabsorption cross sections. But many experimental challenges remain and it is not likely to be studied with the present-day third-generation synchrotron light sources. Resolution of light sources approaching those in lasers would be needed for such an investigation. From the theoretical side, however, the present version of the HSCC is expected to be capable of calculating the Ericson fluctuations. With a little more effort, we expect that calculation of the photoabsorption cross sections above the  $N=9$  threshold to, say,  $N=20$  or  $25$  would be possible. It would be interesting to convince ourselves that indeed Ericson fluctuations are observed in the region where the NNS approaches the Wigner distribution.

Before closing, it is appropriate to address where to go from here. First, the calculation of spectra, either in electron- $\text{He}^+$  collisions, or in photoabsorption cross section from the ground state of He, should be carried out. The levels calculated in this paper will appear as clearly separated resonances in the low- $N$  region, and it would be interesting to see how the Ericson fluctuations emerge as one approaches the high- $N$  region. Such calculations are expected to be straightforward since this amounts to the solution of the coupled hyperradial equations only. With the number of channels truncated to several tens only (see Fig. 3 or 4), the computation effort is small even if we have to scan a range of energy with dense points.

Second, it is tempting to speculate, and to be confirmed by real calculations in the future, a connection between quantum chaos and the Wannier threshold law for double ionization. While it is generally “believed” that the Wannier threshold law [20] is the correct asymptotic theory for double escape of two electrons near threshold from an ionic core, its region of validity has never been established and controversy [64] continued to appear when experimental cross sections are analyzed [65,66]. The channels included in the analysis of quantum chaos are the channels believed to contribute to the two-electron escape. We anticipate a cross correlation between the rate of approaching quantum chaos (such as the Brody parameter  $q \rightarrow 1$ ) and the exponent of the Wannier

threshold law. When the rate of reaching the Wigner distribution is slower, the corresponding Wannier exponent is also smaller. We have no quantitative results to support this argument yet. However, among all the NNS studied in this paper, those systems or symmetries that have slower rates of reaching the  $q=1$  limit are those with small Wannier exponents. The Wannier threshold law has a long history and many tens of theoretical and experimental papers have been devoted to this subject [67–70]. Since previously no theoretical or experimental papers can handle the energy region within less than 0.1 eV (scaled) from the double ionization threshold, most of the discussions of the region of validity of Wannier threshold law is qualitative.

With the present HSCC method, we believe that it is possible to carry out realistic calculations down to 0.03 or 0.04 eV from the threshold for the electron impact ionization of atomic hydrogen. Within the HSCC framework, such calculations have been carried out previously by Kato and Watanabe [41] for electron impact ionization of atomic hydrogen without the truncation of channels. Using up to about 100 channels they could include channels only up to  $I_5$  or  $I_6$  region, or at an energy of about 0.5 eV from the double electron escape threshold. At 0.5 eV below the double escape threshold, the signature of quantum chaos is quite limited. Using the truncated set of channels, we can carry out the calculation to energies much closer to the two-electron escape threshold. We note that new theoretical tools [71–75] for treating double ionization have emerged since the work of Kato and Watanabe. Still, it is very difficult to reach energies very close to the two-electron escape threshold without the truncation of channels employed in the present paper. We note that in the most recent study of the threshold law in  $e$ -H ionizing collisions [76], the lowest collision energy is still 0.27 eV from the threshold. For the bound states, this would correspond to  $I_7$  for  $\text{H}^-$ . In this region, the effect of channel interaction is weak and no quantum chaos is expected. It would be desirable to extend the present HSCC approach, to repeat the calculation in the low energy region as in these studies and then to energies even closer to the two-electron escape threshold. Such calculations, of course, would require additional numerical development.

#### ACKNOWLEDGMENTS

This work was supported in part by the Chemical Sciences, Geosciences and Biosciences Division, Office of Basic Energy Sciences, Office of Science, U. S. Department of Energy. T.M. was supported in part by a Grant-in-Aid for Scientific Research (C) from the MEXT, Japan, by the 21st Century COE program on Coherent Optical Science, and by Matsuo foundation.

- 
- [1] O. Bohigas, M.-J. Giannoni, and C. Schmit, *Phys. Rev. Lett.* **52**, 1 (1984).  
 [2] E. P. Wigner, in *Proceedings of the Fourth Canadian Mathematical Congress*, edited by M. S. MacPhail (University of

- Toronto Press, Toronto, 1959), p. 174 [reprinted in *Statistical Theories of Spectra*, edited by C. E. Porter (Academic, New York, 1968)].  
 [3] F. J. Dyson and M. L. Mehta, *J. Math. Phys.* **4**, 701 (1963).

- [4] M. L. Mehta, *Random Matrices* (Academic, New York, 1991).
- [5] F. Haake, *Quantum Signature of Chaos* (Springer, Berlin, 1991).
- [6] T. Guhr, A. Müller-Groeling, and H. A. Weidenmüller, *Phys. Rep.* **299**, 189 (1998).
- [7] H. Friedrich and D. Wintgen, *Phys. Rep.* **183**, 37 (1989).
- [8] C. H. Iu, G. R. Welch, M. M. Kash, L. Hsu, and D. Kleppner, *Phys. Rev. Lett.* **63**, 1133 (1989).
- [9] J. W. Cooper, U. Fano, and F. Prats, *Phys. Rev. Lett.* **10**, 518 (1963).
- [10] C. D. Lin, *Adv. At. Mol. Phys.* **22**, 77 (1986).
- [11] R. Püttner, B. Gremaud, D. Delande, M. Domke, M. Martins, A. S. Schlachter, and G. Kaindl, *Phys. Rev. Lett.* **86**, 3747 (2001).
- [12] R. Blümel and W. P. Reinhardt, in *Quantum Chaos*, edited by G. Casati and B. V. Chirikov (Cambridge University Press, Cambridge, England, 1995), p. 301.
- [13] R. Blümel and W. P. Reinhardt, *Chaos in Atomic Physics* (Cambridge University Press, Cambridge, England, 1997).
- [14] J. P. Connerade, I. P. Grant, P. Marketos, and J. Oberdisse, *J. Phys. B* **28**, 2539 (1995).
- [15] V. V. Flambaum, A. A. Gribakina, and G. F. Gribakin, *Phys. Rev. A* **58**, 230 (1998).
- [16] N. Vaeck and N. J. Kylstra, *Phys. Rev. A* **65**, 062502 (2002).
- [17] M. Courtney and D. Kleppner, *Phys. Rev. A* **53**, 178 (1996).
- [18] H. Held and W. Schweizer, *Phys. Rev. Lett.* **84**, 1160 (2000).
- [19] J. M. G. Gomez, R. A. Molina, A. Relano, and J. Retamosa, *Phys. Rev. E* **66**, 036209 (2002).
- [20] G. H. Wannier, *Phys. Rev.* **90**, 817 (1953).
- [21] R. P. Madden and K. Codling, *Phys. Rev. Lett.* **10**, 516 (1963).
- [22] P. L. Altick and E. Neal Moore, *Phys. Rev. Lett.* **15**, 100 (1965).
- [23] D. R. Herrick and O. Sinanoglu, *Phys. Rev. A* **11**, 97 (1975).
- [24] C. D. Lin, *Phys. Rev. A* **29**, 1019 (1984).
- [25] M. Domke, K. Schulz, G. Remmers, A. Gutierrez, G. Kaindl, and D. Wintgen, *Phys. Rev. A* **51**, R4309 (1995).
- [26] D. R. Herrick and M. E. Kellman, *Phys. Rev. A* **21**, 418 (1980).
- [27] J. M. Feagin and J. S. Briggs, *Phys. Rev. A* **37**, 4599 (1988).
- [28] M. Aymar, C. H. Greene, and E. Luc-Koenig, *Rev. Mod. Phys.* **68**, 1015 (1996).
- [29] G. Tanner, K. Richter, and J.-M. Rost, *Rev. Mod. Phys.* **72**, 497 (2000).
- [30] J.-Z. Tang, S. Watanabe, M. Matsuzawa, and C. D. Lin, *Phys. Rev. Lett.* **69**, 1633 (1992).
- [31] B. Gremaud and D. Delande, *Europhys. Lett.* **40**, 363 (1997).
- [32] M. Domke, K. Schulz, G. Remmers, G. Kaindl, and D. Wintgen, *Phys. Rev. A* **53**, 1424 (1996).
- [33] S. I. Themelis, Y. Komninos, and C. A. Nicolaides, *Eur. Phys. J. D* **18**, 277 (2002).
- [34] T. Ericson, *Phys. Rev. Lett.* **5**, 430 (1960).
- [35] R. Blümel, *Phys. Rev. A* **54**, 5420 (1996).
- [36] C. D. Lin, *Phys. Rep.* **257**, 1 (1995).
- [37] C. N. Liu, A. T. Le, T. Morishita, B. D. Esry, and C. D. Lin, *Phys. Rev. A* **67**, 052705 (2003).
- [38] J. C. Light, I. P. Hamilton, and J. V. Lill, *J. Chem. Phys.* **82**, 1400 (1985).
- [39] O. I. Tolstikhin, S. Watanabe, and M. Matsuzawa, *J. Phys. B* **29**, L389 (1996).
- [40] K. I. Hino, A. Igarashi, and J. H. Macek, *Phys. Rev. A* **56**, 1038 (1997).
- [41] D. Kato and S. Watanabe, *Phys. Rev. A* **56**, 3687 (1997).
- [42] O. I. Tolstikhin and H. Nakamura, *J. Chem. Phys.* **108**, 8899 (1998).
- [43] T. Morishita, K. Hino, T. Edamura, D. Kato, S. Watanabe, and M. Matsuzawa, *J. Phys. B* **34**, L475 (2001).
- [44] T. Morishita, T. Sasajima, S. Watanabe, and M. Matsuzawa, *Nucl. Instrum. Methods Phys. Res. B* **214**, 144 (2004).
- [45] A. T. Le, C. N. Liu, and C. D. Lin, *Phys. Rev. A* **68**, 012705 (2003).
- [46] A. T. Le, M. Hesse, T. G. Lee, and C. D. Lin, *J. Phys. B* **36**, 3281 (2003).
- [47] T. G. Heil, S. E. Butler, and A. Dalgarno, *Phys. Rev. A* **23**, 1100 (1981).
- [48] M. Hesse, A. T. Le, and C. D. Lin, *Phys. Rev. A* **69**, 052712 (2004).
- [49] A. T. Le and C. D. Lin, *Phys. Rev. A* **71**, 022507 (2005).
- [50] T. G. Lee, M. Hesse, A. T. Le, and C. D. Lin, *Phys. Rev. A* **70**, 012702 (2004).
- [51] S. S. M. Wong and J. B. French, *Nucl. Phys.* **198**, 188 (1972).
- [52] R. Venkataraman, *J. Phys. B* **15**, 4293 (1982).
- [53] T. A. Brody, J. Flores, J. B. French, P. A. Mello, A. Pandey, and S. S. M. Wong, *Rev. Mod. Phys.* **53**, 385 (1981).
- [54] H. Fukuda, N. Koyama, and M. Matsuzawa, *J. Phys. B* **20**, 2959 (1987).
- [55] N. Koyama, A. Takafuji, and M. Matsuzawa, *J. Phys. B* **22**, 553 (1989).
- [56] H. R. Sadeghpour, *Phys. Rev. A* **43**, 5821 (1991).
- [57] G. Handke, M. Draeger, and H. Friedrich, *Physica A* **197**, 113 (1993).
- [58] M. Draeger, G. Handke, W. Ihra, and H. Friedrich, *Phys. Rev. A* **50**, 3793 (1994).
- [59] J. Zakrzewski, K. Dupret, and D. Delande, *Phys. Rev. Lett.* **74**, 522 (1995).
- [60] X. H. Liu, Z. Chen, and C. D. Lin, *Phys. Rev. A* **44**, 5468 (1991).
- [61] K. Richter, G. Tanner, and D. Wintgen, *Phys. Rev. A* **48**, 4182 (1993).
- [62] O. Bohigas *et al.*, in *Nuclear Data for Science and Technology*, edited by K. H. Böchhoff (Reidel, Dordrecht, 1983), p. 809.
- [63] F. S. Stephens, M. A. Deleplanque, I. Y. Lee, A. O. Macchiavelli, D. Ward, P. Fallon, M. Cromaz, R. M. Clark, M. Descovich, R. M. Diamond, and E. Rodriguez-Vieitez, *Phys. Rev. Lett.* **94**, 042501 (2005).
- [64] A. Temkin, *Phys. Rev. Lett.* **49**, 365 (1982).
- [65] J. R. Friedman, X. Q. Guo, M. S. Lubell, and M. R. Frankel, *Phys. Rev. A* **46**, 652 (1992).
- [66] D. Lukic, J. B. Bluett, and R. Wehlitz, *Phys. Rev. Lett.* **93**, 023003 (2004).
- [67] A. R. P. Rau, *Phys. Rev. A* **4**, 207 (1971).
- [68] J. H. Macek and S. Yu. Ovchinnikov, *Phys. Rev. A* **50**, 468 (1994).
- [69] J. M. Feagin, *J. Phys. B* **17**, 2433 (1984).
- [70] J.-M. Rost, *Phys. Rev. Lett.* **72**, 1998 (1994).
- [71] C. W. McCurdy, M. Baertschy, and T. N. Rescigno, *J. Phys. B* **37**, R137 (2004).
- [72] T. N. Rescigno, M. Baertschy, W. A. Isaacs, and C. W. McCurdy, *Science* **286**, 2474 (1999).

- [73] L. Malegat, P. Selles, and A. K. Kazansky, Phys. Rev. Lett. **85**, 4450 (2000).  
[74] P. Selles, L. Malegat, A. Huetz, A. K. Kazansky, S. A. Collins, D. P. Seccombe, and T. J. Reddish, Phys. Rev. A **69**, 052707 (2004).  
[75] I. Bray, Phys. Rev. Lett. **89**, 273201 (2002).  
[76] P. L. Bartlett and A. T. Stelbovics, Phys. Rev. Lett. **93**, 233201 (2004).